Coaxial transfer orbit between non-coplanar and non-coaxial elliptical orbits

Elvis Lacruz *
Center for Physics Studies of the Cosmos of Aragon, Teruel, Spain, 44001
Dept. of Mathematics, Valencian International University, Valencia, Spain, 46002

Ángeles Dena†
Defense University Center in Zaragoza, Zaragoza, Spain, 50090

Nomenclature

(Nomenclature entries should have the units identified)

μ	=	standard gravitational parameter, km^3/s^2.
$\mathbf{v}$ and V	=	velocity vector and its magnitude, km/s.
$\Delta\mathbf{v}$ and Δv	=	differences between two instantaneous velocities and its magnitude, km/s.
ΔV	=	characteristic velocity, km/s.
r_{p_i}, r_{p_f}, r_{p_t}, r_{a_i}, r_{a_f}, r_{a_t}	=	initial, final and transfer periapsis and apoapsis, km.
σ_k	=	set of six variables, with $k = \{i, j, t\}$.
a	=	semimajor axis, km.
e	=	eccentricity.
i	=	inclination, degrees.
Ω	=	right ascension node, degrees.
ω	=	argument of periapis, degrees.
ν	=	true anomaly, degrees.
θ	=	angular distance, degrees.
O_i, O_t and O_f	=	initial, final and transfer orbits.
Π_i, Π_f and Π_t	=	initial, final and transfer orbital planes.
$\boldsymbol{n}$ and $\boldsymbol{\ell}$	=	the line of nodes and the line of apsides.

*Professor - Telescope Operator, Department Scientific Operation DOPC, elacruz@cefca.es, and AIAA Member Grade (if any) for first author.
†Associate Professor, APEDIF — Instituto Universitario de Matemáticas y Aplicaciones.

$\mathcal{P}_{\mathcal{F}}$ = Parametric function.

c_j = coefficients $j = \{0, 1, \cdots, 7\}$.

Subscripts

i, f and t = initial, final, and transfer.

I. Introduction

There is an ever-increasing number of orbiters (satellites, space probes, space debris, and others) around the celestial bodies of the Solar System, in particular of the Earth. European Space Agency (ESA) has statistically estimated [1], that more than 330 million objects (between 1 cm until 50 m) are in orbit around our planet [2]. About 35.000 are catalogued by tracking from ground-based optical and radar sensors [3–5]. Deploying space missions in Low Earth Orbit (LEO), Medium Earth Orbit (MEO) and Geostationary Equatorial Orbit (GEO) has become more complicated because since the beginning of the space age, space debris has been increasing every day, particularly with the recent launching of large constellations [6]. These three regions present new complex scenarios to send and hold new orbiters into orbit, re-position spacecraft, or capture and remove orbiters. One of the feasible solutions is to apply an active space debris removal method [7], e.g. satellite-based methods involving key technologies such as arms control, approach, rendezvous, orbit changes and capture [8]. Another possibility is to change the trajectory of the space mission to avoid possible collisions with space debris and launch traffic. In all these cases, trajectory changes are achieved by distribution forces or orbital maneuvers. Many configurations of the orbital transfer problem have been analyzed and studied to determine the most effective and optimal possible maneuver. The first of such studies started in the 1920s with the pioneering work by Hohmann [9], who conjectured that the minimum fuel transfer between coplanar circular orbits is the bi-tangent elliptic transfer performed through two tangential impulsive changes of velocity, which occur at the apse points of the transfer orbit. Such transfer is referred to as the Hohmann transfer, and for a relatively long time, it was assumed to be globally optimal in terms of total velocity change. However, in the late 1950s and coinciding with the Soviet Luna 2 spacecraft launch - the first space vehicle to perform orbital maneuvers while approaching the Moon - significant advances in the investigation of impulsive trajectories were carried out by Shternfeld, Edelbaum and Hoelker [10–12].

In the early 1960s, Ting [13] proved the local optimality of the Hohmann transfer and stated that the optimal orientation of the axes is coaxial and aligned for the initial and final elliptical orbits. Ting [13] also demonstrated that

the minimum cost transfer corresponds to coplanar initial, final, and transfer orbits. The same author also proved that orbital transfers performed through four or more impulses are never optimal [14]. Subsequently, the optimality of the Hohmann transfer was proved using different tools.

Lawden [15, 16] and Barrar [17] first proved the global optimality of the Hohmann transfer with two impulse transfers, then Marec [18], Battin [19], Palmore [20] and Prussing [21] presented elementary proofs about this. Additionally, Moyer [22] demonstrated the global optimality of Hohmann and bi-elliptic transfers from a circular to an elliptic orbit without restrictions on the number of impulses. A little over a decade ago, Pontani [23] proposed a simple, original approach to determine the global optimal impulsive transfers between two coplanar trajectories, without any restriction on the number of impulses and with some constraints on the radius of the closest approach or greatest recession.

In the last century, the main true goal has been to minimize propellant expenditure. A velocity impulse approximates the effect of the propulsive thrust, by assuming that an instantaneous velocity change can occur (while the spacecraft position remains unchanged). The impulsive approximation has applications in the case of high-thrust rockets and spacecraft, and represents a very accurate approximation of the finite–thrust maneuvers that a vehicle performs once it is in orbit, under the assumption that gravitational losses during propulsion can be neglected [24, 25].

Many cases have been studied and evaluated taking into account restrictions coupled with the formulation of the problem. The fundamental reason for this is bounded by the fact that each case is unique, identified both by its formulation and its constraints. The most fundamental transfer problems are those known as Hohmann transfer, bi-elliptical transfer, and/or Lambert problem transfer [26–28]. Recently the classical problem of two-impulse optimal co-tangential transfer between two coplanar elliptic orbits has been analyzed assuming changes only in the directions of the velocity [29].

The general goal of this Note is to calculate, analytically and numerically, the minimum characteristic velocity, ΔV, when the initial and final orbits are non-coplanar and non-coaxial elliptical orbits, using a transfer orbit that is coaxial with either the initial or the final orbit, with no restriction on its being coplanar with either. For it, the aim is to obtain an optimal width region from the smallest possible number of orbital elements and to compute a parametric function derived from the most efficient configuration in terms of the semimajor axis and the eccentricity.

This Note is organized as follows: In Sec. II a description of the problem and the constraints required are given. In Sec. II.A we derive a function for the ΔV of the two impulsive maneuvers, to make an analytical study of four basic

configurations possibles. This function is determined and reduced to only two orbital elements of the generated transfer orbit. In addition, we calculate analytical expressions for the partial derivatives in each variable and configuration. In Sec. III we consider sets of orbital elements from real data to evaluate numerically the function of the ΔV, estimate the best configuration and determine the optimal width region. Finally, in Sec. IV we present the most relevant contributions obtained with this study.

II. Model Formulation and constraints

Without loss of generality, we assume that an orbiter (e.g. spacecraft, satellite, space debris, space probe) is modeled as a point mass object on which the Newtonian gravitational force acts and relativistic effects are neglected. Moreover, the 3D orbital transfer problem is considered so that, the initial and final orbits are non-coplanar and non-coaxial elliptical orbits. Fig. 1 shows a sketch of the general formulation, the inner initial orbit in blue and the outer final one in red, respectively. Therefore, the semimajor axes are $a_i < a_f$. By Kepler's law, all orbits have a common focus located at the origin, O, of the inertial reference frame $\{O, \boldsymbol{x}, \boldsymbol{y}, \boldsymbol{z}\}$.

One of the ways to represent an orbit is through the classical orbital elements, that is by six variables $\sigma_k = \{a_k, e_k, i_k, \Omega_k, \omega_k, \nu_k\}$, where a_k represents the semimajor axis, e_k the eccentricity, i_k the inclination, Ω_k the right ascension of the ascending node, ω_k the argument of periapsis and ν_k the true anomaly. In this work, we consider three orbits: the initial, the final and the transfer orbit so, σ_k with $k = i, f$, an t_j, respectively. We represent each set as a symbolic function $O(\sigma_k) = O_k$, which is implicitly related to the orbit. The subscript j designates the jth-transfer orbit involved in the entire transfer process. In the general case, the existence of a finite number of transfer orbits is contingent upon the number of instantaneous maneuvers that can be applied, under specified restrictions, to facilitate the transition from the initial to the final orbits.

Figure 1 shows the O_i (blue color) and O_f (red color) that represent the initial and final elliptical orbits, respectively referred to $\{O, \boldsymbol{x}, \boldsymbol{y}, \boldsymbol{z}\}$. The model formulation is devised such that each orbit is situated within a 2-dimensional hyperplane or orbital plane, denoted by Π_i and Π_f respectively, as illustrated in Fig. 1. Geometrically, these orbital planes are non-coplanar, so there is an intersection line between them defined by the vector $\boldsymbol{n}_{if}$, which is the vertex of the dihedral angle between both planes. This angle is confined to the interval $0° < i_{fi} \leq 90°$ and can be determined by the difference between the angles i_f and i_i under the condition that i_i is less than i_f. As a direct consequence of the formulation, the line of apsides and nodes are defined by the vectors $\boldsymbol{\ell}_i$, $\boldsymbol{\ell}_f$, $\boldsymbol{n}_i$ and $\boldsymbol{n}_f$, respectively. A way to

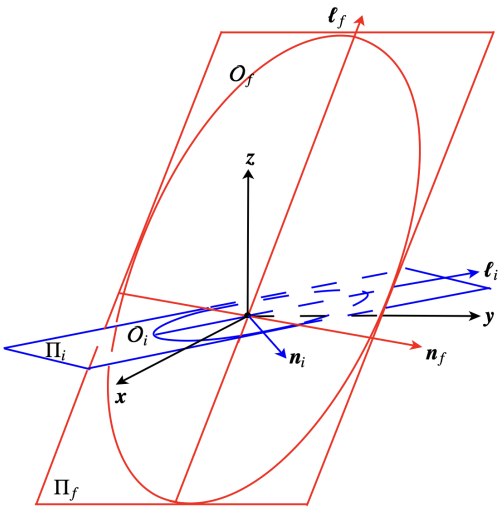

Fig. 1 Geometry of the 3D-orbital transfer between non-coplanar and non-coaxial elliptical orbits.

maneuver a satellite or spacecraft is through a combined sequence of discrete coplanar (tangential) and non-coplanar (non-tangential) instantaneous impulsive maneuvers that allow an orbiter to make a change between orbits. With the application of coplanar impulses is possible to modify the orbit's shape and size; i.e: semimajor axis, eccentricity, as well as the argument of periapsis. Additionally, the orbit's orientation can be changed by varying the inclination and right ascension of the ascending node [27]. This is one of the features of the Astrodynamics, that allows for designing and defining orbits by modifying their geometry and orientation [30]. There are many possibilities bounded only by the complexity of the problem. Herein, two combined impulsive maneuvers are considered and studied in the model formulation as constrains.

A. Characteristic velocity ΔV

The function, ΔV, measures the total of the velocity change that an orbiter needs to change from one orbit to another. This cost, which is the characteristic velocity, includes all applied maneuvers. In other words, the ΔV is the sum of instantaneous $N-$impulses, which is defined by:

$$\Delta V = \sum_{l=1}^{N} \Delta v_l, \tag{1}$$

where, Δv_l is the magnitude of the differences between two instantaneous velocities. The subscript $l = 1, 2, \ldots, N$ represents the number of the applied impulsive maneuvers. Keeping in mind that the velocity in the departure and arrival points is denoted by the vectors $\mathbf{v}_i$ and $\mathbf{v}_f$, respectively, their magnitudes are V_i and V_f, then the $\Delta v_l = |V_f - V_i|$. In this sense, we take into account two discrete impulsive maneuvers. Therefore, the Eq. (1) simply becomes:

$$\Delta V = \Delta v_1 + \Delta v_2, \tag{2}$$

thus, the $jth-$transfer orbit associated with two applied impulsive maneuvers is O_{t_1}, which for simplicity we denote as O_t. This orbit is treated as a combination of coplanar and non-coplanar impulsive maneuvers that can be an orbit coplanar or not, and coaxial or not, with either the initial or the final orbit. This situation translates into two possibilities. Firstly, the O_t is coplanar and coaxial with either O_i or O_f and secondly, the O_t is non-coplanar and coaxial with either O_i or O_f. In this context, we consider two orbits to be coaxial if the vector resulting from the cross product between the vectors defining the lines of apsides points in the same direction. If this vector is null, the orbits are coaxial and, specifically, coplanar, with their directions determined by the nodes. In the next subsections, we study each case separately taking into account the constraints that arise.

B. Configuration where the O_t is coplanar and coaxial with O_i

This configuration is illustrated in Fig. 2, representing the geometry with respect to $\{O, \boldsymbol{x}, \boldsymbol{y}, \boldsymbol{z}\}$. Additionally, it shows the representation of vector components associated with impulsive maneuvers, namely $\Delta\mathbf{v}_1$ and $\Delta\mathbf{v}_2$, applied at the points of departure and arrival, respectively. The first impulsive maneuver is coplanar with the orbital plane, Π_i, i.e. $\Delta\mathbf{v}_1 \in \Pi_i$ preserves the direction and increases only the magnitude of the velocity, V_i, in the point of the departure of the orbiter, that is located in the initial orbit. By construction, this orbit should arrive at a point in the final orbit. The second impulsive maneuver is non-coplanar with the Π_f, i.e. $\Delta\mathbf{v}_2 \notin \Pi_f$, which is needed to change the direction, and thus the orbiter is transferred to the final orbit. As the $\Delta\mathbf{v}_2$ is non-tangential it induces a dihedral angle, denoted as θ_{tf}, situated between the planes Π_i and Π_f. This angle together with i_i, i_f, Ω_i and Ω_f, forms a spherical triangle as shown in the Fig. 3.

As the initial and transfer orbits are coplanar and coaxial, the lines of nodes and apsides are equivalents i.e. $\boldsymbol{n}_i = \boldsymbol{n}_t$ and $\boldsymbol{\ell}_i = \boldsymbol{\ell}_t$, respectively. Consequently, the true anomalies are same ($\nu_i = \nu_t$). Then, the angular distance, θ_{tf}, has a solution in function of the orbital elements of the initial and final orbits. With this configuration, there are several cases in which the first impulsive maneuver can be applied: 1) the periapsis of the initial orbit, r_{p_i}, and apoapsis of the transfer orbit, r_{a_t}, are equal, $r_{p_i} = r_{a_t}$; 2) the periapsis of both orbits are equal, $r_{p_i} = r_{p_t}$; and 3) the apoapsis of both orbits are equal, $r_{a_i} = r_{a_t}$. The first and third cases are not taken into account. In this first case, the model formulation assumes that the initial orbit is smaller than the final orbit, giving rise to the condition $r_{p_i} = r_{a_t} > r_{p_t}$ and therefore $O_i > O_t$, which is a contradiction. Besides, this case is not possible because the transfer orbit would not have a point in

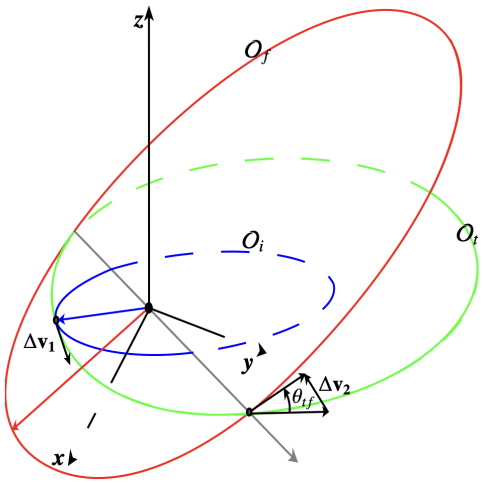

Fig. 2 Geometry of the transfer: O_t (green) is coplanar and coaxial with O_i (blue).

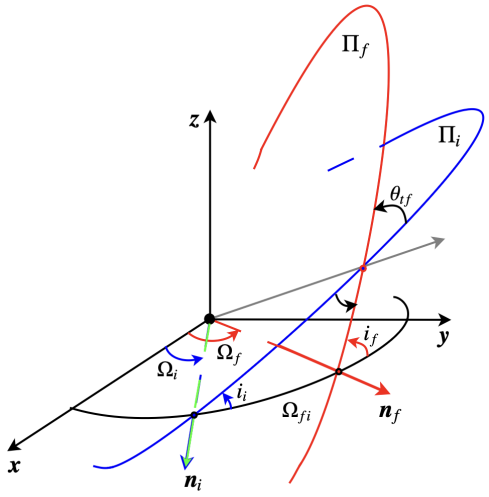

Fig. 3 Geometry relation of θ_{tf} as a function of i_i, i_f, Ω_i and Ω_f.

common with the final orbit. Concerning the third case the maneuver is more expensive in the apoapsis than in the periapsis [19]. Therefore, only the second case is considered and the Δv_1 is applied in the periapsis of initial and transfer orbits, as shown in Fig. 2. The Δv_2 is applied to change from the transfer orbit to the final orbit, and this maneuver is more expensive that the first one since it requires changing planes.

Taking into account the law of conservation of energy, angular momentum and Kepler's equation, [19, 27, 30] Eq. (2) that represents the ΔV is defined as:

$$\Delta V = \left(V_{O_t} - V_{O_i}\right) + \sqrt{V_{O_t}^2 + V_{O_f}^2 - 2\,V_{O_t}\,V_{O_f}\,\cos\theta_{tf}}, \tag{3}$$

where, V_{O_i}, V_{O_t} and V_{O_f} are the velocity magnitudes of the initial, transfer, and final orbits, respectively. The angle θ_{tf} is measured between the planes Π_t and Π_f, or it is equivalent to angle between Π_i and Π_f. Then, these velocities are expressed in term of the orbital elements of the initial and transfer orbits. Substituting in Eq. (3), taking into account the above constrains, making some reductions, and rearranging terms, we obtain a ΔV function as follows:

$$\Delta V = \sqrt{\mu}\left[\sqrt{\alpha_t} - \sqrt{\alpha_i} + \sqrt{\delta_f + \delta_{it} - 2\sqrt{\delta_f \delta_{it}}\,\cos\theta_{tf}}\right], \tag{4}$$

where, μ is the standard gravitational parameter, determined by the gravitational constant and the mass of the central body. The quantities α_t, α_i, δ_f and δ_{it} are defined by;

$$\alpha_t = \frac{1+e_t}{a_t(1-e_t)}, \quad \alpha_i = \frac{1+e_i}{a_i(1-e_i)}, \quad \delta_f = \frac{(e_f+\cos\nu_f)^2+\sin^2\nu_f}{a_f(1-e_f^2)} \quad \text{and} \quad \delta_{it} = \frac{(e_t+\cos\nu_i)^2+\sin^2\nu_i}{a_t(1-e_t^2)}.$$

These variables have a solution as long as the eccentricity, e_t, is less than unity, i.e. the transfer orbit is neither parabolic

nor hyperbolic. Furthermore, the semimajor axes of the orbits are not null.

The angle θ_{tf} corresponds to the dihedral angle between Π_i and Π_f and it one of the three angles constituting the spherical triangle depicted in Fig. 3. According to the law of cosines, θ_{tf} is determined by $\theta_{tf} = \cos^{-1}[\cos i_i \cos i_f - \sin i_i \sin i_f \cos \Omega_{fi}]$, with $\Omega_{fi} = \Omega_f - \Omega_i$.

Equation (4) is reduced to two unknown orbital elements: the semimajor axis, a_t, and eccentricity, e_t, of the transfer orbit. This represents an advantage since the set the unknown variables is reduced to two, as the other variables are known from the initial conditions of the model formulation. It is possible to calculate values for a_t and e_t such that the ΔV is minimal. Thus, we obtain the following analytical expressions once the terms have been simplified, that is, the partial derivatives with respect to each variable are:

$$\partial \Delta V_{a_t} = \frac{\sqrt{\mu}}{2\, a_t\, \xi_1} \left[\xi_2 - (\xi_1 \sqrt{\alpha_t} + \delta_{it}) \right], \quad \text{and} \tag{5}$$

$$\partial \Delta V_{e_t} = \frac{\sqrt{\mu}}{(1 - e_t^2)} \left[- \frac{\sqrt{\alpha_t}\, \delta_f\, \xi_1}{\xi_2} + \left(\delta_f \cos \theta_{tf} - \xi_2 \right) \left(2e_t + (1 + e_t^2) \cos \nu_i \right) \right], \tag{6}$$

where the new quantities ξ_1 and ξ_2 are defined by $\xi_1 = \sqrt{\delta_f + \delta_{it} - 2\,\xi_2}$ and $\xi_2 = (\delta_f\, \delta_{it})^{1/2} \cos \theta_{tf}$. It is possible to examine and determine values for these quantities, which depend on the values of the ten orbital elements, such as: a_i, e_i, i_i, Ω_i, ν_i, a_f, e_f, i_f, ν_f and Ω_f. Addition constraints are established by the fact that $\xi_1 > 0$ and $\xi_2 > 0$.

C. Configuration where the O_t is coplanar and coaxial with O_f

With this configuration, to transfer an orbiter from the initial to final orbit the applied impulsive maneuvers are such that; $\Delta \mathbf{v}_1$ is non-tangential impulsive maneuver applied in the point of departure, $\Delta \mathbf{v}_1 \notin \Pi_i$, and $\Delta \mathbf{v}_2$ is tangential impulsive maneuver applied in the point of arrival, $\Delta \mathbf{v}_2 \in \Pi_f$. Assuming that the O_t (green color) is coplanar and coaxial with O_f (red color), therefore the lines of nodes and apsides are equivalents i.e. $\boldsymbol{n}_t = \boldsymbol{n}_f$ and $\boldsymbol{\ell}_f = \boldsymbol{\ell}_t$, respectively. Consequently, the true anomalies are same ($\nu_f = \nu_t$). In Fig. 4, the geometry of the transfer is shown, from initial to final orbit. $\Delta \mathbf{v}_1$ is non-tangential, so it generates a dihedral angle, θ_{it}, between the initial and transfer orbital planes. This angle is determined by i_i, i_f, Ω_i and Ω_f as the previous angle θ_{tf}. Analogously to the previous configuration, the maneuvers are calculated in terms of the orbital elements involved in this problem. The impulsive maneuvers are applied at a common point of both orbits. The first impulsive maneuver changes the direction of the orbital velocity and therefore the hyperplane, while the second impulse only changes the magnitude of the orbital velocity (increasing it) but preserving its direction. Nevertheless, there are several cases where the second impulse maneuver can be applied: (1) if

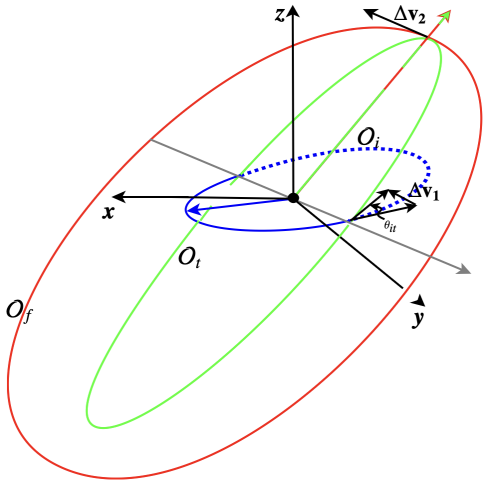

Fig. 4 Geometry of the transfer: O_t (green) is coplanar and coaxial with O_f (red).

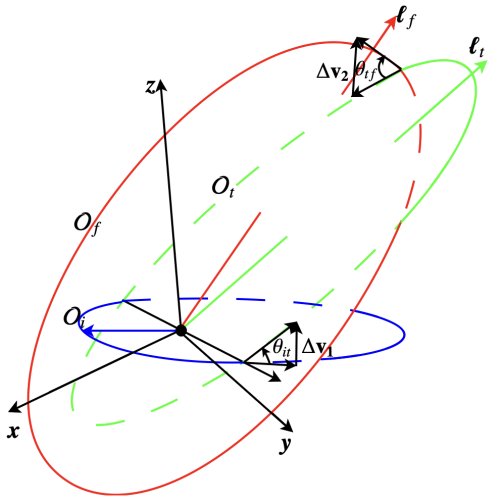

Fig. 5 Geometry of the transfer: O_t (green) is non-coplanar and coaxial with O_i (blue) and non-coaxial with O_f (red).

the periapsis of the final orbit, r_{p_f}, and apoapsis of the transfer orbit, r_{a_t}, are equal ($r_{p_f} = r_{a_t}$), (2) if the periapsis of both orbits are equal ($r_{p_f} = r_{p_t}$) and (3) if the apoapsis of both orbits are equal ($r_{a_f} = r_{a_t}$). This configuration is considered only when the $r_{p_f} = r_{p_t}$ since at this point the maneuvers are less expensive [19]. Note that the first case does not hold because the relation $r_{a_f} < r_{p_t}$ does not occur. Thus, is:

$$\Delta V = \sqrt{V_{O_t}^2 + V_{O_i}^2 - 2\,V_{O_t}\,V_{O_i}\,\cos\theta_{it}} + \left(V_{O_f} - V_{O_t}\right), \tag{7}$$

which is a function similar to the Eq. (3). Thus, this is:

$$\Delta V = \sqrt{\mu}\left[\sqrt{\delta_{tf} + \delta_i - 2\sqrt{\delta_{tf}\delta_i}\,\cos\theta_{it}} + \sqrt{\alpha_f} - \sqrt{\alpha_t}\right], \tag{8}$$

where, the quantities δ_{tf}, δ_i and α_f are defined by;

$$\delta_{tf} = \frac{(e_t + \cos\nu_f)^2 + \sin^2\nu_f}{a_t\,(1-e_t^2)}, \quad \delta_i = \frac{(e_i + \cos\nu_i)^2 + \sin^2\nu_i}{a_i\,(1-e_i^2)}, \quad \text{and} \quad \alpha_f = \frac{1+e_f}{a_f\,(1-e_f)}.$$

The angle θ_{it} represents the dihedral angle between the velocity vectors $\mathbf{v}_i$ and $\mathbf{v}_t$. Given that O_t is coplanar and coaxial with O_f, this angle constitutes one of the angles in a spherical triangle involving i_i, i_f, and $\Omega_{fi} = \Omega_f - \Omega_i$, therefore, $\theta_{it} = \cos^{-1}[\cos i_i\,\cos i_f - \sin i_i\,\sin i_f\,\cos\Omega_{fi}]$. Since the final and transfer orbits are coaxial, then $\nu_t = \nu_f$. Equivalently to the previous configuration, it is possible to obtain expressions for the partial derivatives, which are determined exclusively in terms of the a_t and e_t, such that:

$$\partial\Delta V_{a_t} = \frac{\sqrt{\mu}}{2\,a_t\,\zeta_1}\left[\zeta_2 + (\zeta_1\sqrt{\alpha_t} - \delta_{tf})\right], \text{ and} \tag{9}$$

$$\partial \Delta V_{e_t} = \frac{\sqrt{\mu}}{(1-e_t^2)} \left[\frac{\sqrt{\alpha_t}\, \delta_i\, \zeta_1}{\zeta_2\, \cos\theta_{it}} + \left(\delta_i\, \cos\theta_{it} - \zeta_2 \right) \left(2\, e_t + (1+e_t^2)\, \cos\nu_f \right) \right], \tag{10}$$

where, the quantities ζ_1 and ζ_2, are defined as; $\zeta_1 = (\delta_i + \delta_{tf} - 2\,\zeta_2)^{1/2}$ and $\zeta_2 = (\delta_i\, \delta_{tf})^{1/2}\, \cos\theta_{it}$. In these expressions, there are terms from the initial and final orbits. In order to obtain minimum values for the ΔV, the terms α_t, $(\delta_i + \delta_{tf} - 2\,\xi_2)$ and $\delta_i\, \delta_{tf}$ need to be strictly positive to obtain real solutions. The different solutions depend on how the initial and final orbits are defined. The relations between the Eq. (5) and Eq. (9), also Eq. (6) and Eq. (10), differ fundamentally due to the presence of the terms δ_i and δ_f. These equations are not equal because a_i is smaller than a_f.

D. Configurations in which O_t is non-coplanar and coaxial with either O_i or O_f

In these two possible formulations, the third and fourth configurations, the problem takes on another level of complexity, requiring the application of two non-coplanar impulsive maneuvers. First, we study the third configuration where the transfer orbit, O_t is non-coplanar and coaxial with O_i, therefore, the cross product between the lines of apsides $\boldsymbol{\ell}_i$ and $\boldsymbol{\ell}_t$ are in the same plane, and mark the same direction of the $\boldsymbol{n}_i$ or $\boldsymbol{n}_t$. To make a change in the trajectory, it must be taken into account in the general formulation that the $\Delta\mathbf{v}_1 \notin \Pi_{O_i}$ and $\Delta\mathbf{v}_2 \notin \Pi_{O_f}$.

Figure 5 shows the three orbits with respect to the $\{O, \boldsymbol{x}, \boldsymbol{y}, \boldsymbol{z}\}$: the initial orbit (blue color), the transfer orbit (green color) and the final orbit (red color). As impulse maneuvers are non-coplanar, they give rise to two dihedral angles, θ_{it} and θ_{tf}, respectively. Therefore, we calculate the ΔV, which is expressed as Eq. (3) and Eq. (7) by:

$$\Delta V = \sqrt{V_{O_t}^2 + V_{O_i}^2 - 2\, V_{O_t}\, V_{O_i}\, \cos\theta_{it}} + \sqrt{V_{O_f}^2 + V_{O_t}^2 - 2\, V_{O_f}\, V_{O_t}\, \cos\theta_{tf}}. \tag{11}$$

This function is determined by the values of the orbital elements of initial and final orbits. Performing some term reductions, we obtain an expression based on a_t and e_t, as in the previous configurations. Thus,

$$\Delta V = \sqrt{\mu} \left[\sqrt{\delta_{it} + \delta_i - 2\,\psi_1} + \sqrt{\delta_f + \delta_{tf} - 2\,\rho_1} \right], \tag{12}$$

being the quantities,

$$\psi_1 = \sqrt{\delta_i\, \delta_{it}}\, \cos\theta_{it}, \quad \rho_1 = \sqrt{\delta_f\, \delta_{tf}}\, \cos\theta_{tf}, \quad \delta_{it} = \frac{(e_t + \cos\nu_i)^2 + \sin^2\nu_i}{a_t\, (1-e_t^2)},$$

$$\delta_i = \frac{(e_i + \cos\nu_i)^2 + \sin^2\nu_i}{a_i\, (1-e_i^2)}, \quad \delta_f = \frac{(e_f + \cos\nu_f)^2 + \sin^2\nu_f}{a_f\, (1-e_f^2)}, \quad \text{and} \quad \delta_{tf} = \frac{(e_t + \cos\nu_f)^2 + \sin^2\nu_f}{a_t\, (1-e_t^2)}.$$

On the other hand, the angles θ_{it} and θ_{tf} are a function of the eight orbital elements i_i, i_t, i_f, Ω_i, Ω_t, Ω_f, ν_i and ν_f.

Both are related in a single trigonometric function and calculated through two spherical triangles, which are

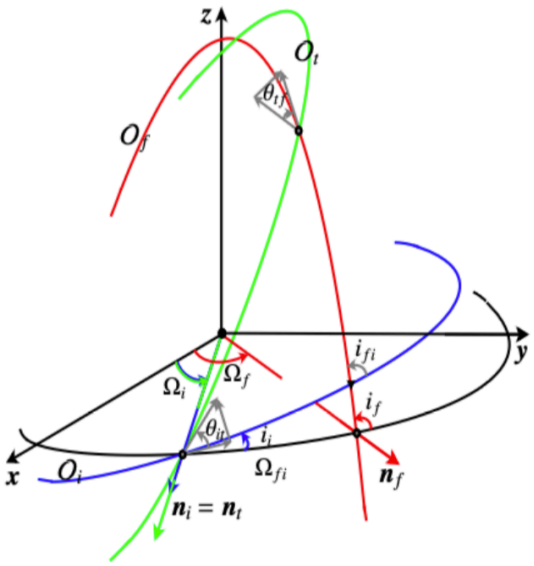

Fig. 6 Geometrical relation between θ_{it} and θ_{tf} with non-tangential impulsive maneuvers $\Delta\mathbf{v_1}$ and $\Delta\mathbf{v_2}$.

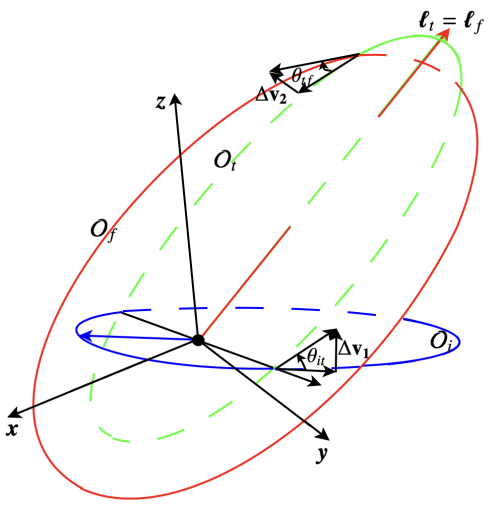

Fig. 7 Geometry of the transfer where O_t (green) is non-coplanar and coaxial with O_f (red).

associated with the angular distances of the initial and final orbits. Figure 6 shows a sketch in which the orbits are projected to highlight the relation between angles. Therefore, through Bessel's formulas, we have that;

$$\theta_{it} = \cos^{-1}\left[\frac{(\gamma\,\cos\phi - \cos\lambda)\,\sqrt{1-\gamma^2}}{\sin\lambda\,(1-\gamma^2)}\right] \quad \text{and} \quad \theta_{tf} = \cos^{-1}\left[\frac{(\cos\phi - \gamma\,\cos\lambda)\,\sqrt{1-\gamma^2}}{\sin\lambda\,(1-\gamma^2)}\right],$$

with $\gamma = \cos\phi\,\cos\lambda - \sin\phi\,\sin\lambda\,\cos i_{fi}$, $\quad \phi = \nu_i - \sin^{-1}\left[\frac{\sin\Omega_{fi}\,\sin i_f}{\sin i_{fi}}\right]$ and $\quad \lambda = \nu_f - \sin^{-1}\left[\frac{\sin\Omega_{fi}\,\sin i_i}{\sin i_{fi}}\right]$.

Thus, the partial derivatives of the Eq. (12) in terms of the a_t and e_t, are:

$$\partial\Delta V_{a_t} = \frac{\sqrt{\mu}}{2a_t\rho_2\psi_2}\left[\psi_2(\rho_1 - \delta_{tf}) + \rho_2(\psi_1 - \delta_{it})\right], \quad \text{and} \tag{13}$$

$$\partial\Delta V_{e_t} = \frac{\sqrt{\mu}\,(\rho_1\,\rho_2\,\psi_1\,\psi_2)^{-1}}{a_t\,(e_t^2-1)^2}\left[[2e_t+(1+e_2^2)\,\cos\nu_f]\,[\rho_1-\cos^2\theta_{tf}\,\delta_f]+[2e_t+(1+e_2^2)\,\cos\nu_i]\,[\psi_1-\cos^2\theta_{it}\,\delta_i]\right] \tag{14}$$

being, $\rho_2 = \sqrt{\delta_f + \delta_{tf} - 2\,\rho_1}$ and $\psi_2 = \sqrt{\delta_i + \delta_{it} - 2\,\psi_1}$. Finally, we study the fourth configuration where O_t is non-coplanar and coaxial with O_f therefore, the direction of the cross product between the lines of apsides $\boldsymbol{\ell}_t$ and $\boldsymbol{\ell}_f$ mark the same that $\boldsymbol{n}_f$ or $\boldsymbol{n}_t$. Analogous to the previous configuration, the impulsive maneuvers $\Delta\mathbf{v_1}$ and $\Delta\mathbf{v_2}$ are non-tangential applied to departure from the initial orbit to arrive at the final orbit, that is, $\Delta\mathbf{v_1} \notin \Pi_{O_i}$ and $\Delta\mathbf{v_2} \notin \Pi_{O_f}$, as shown in Fig. 7. This fact is irrelevant since the maneuvers generate the same angles in both configurations. Therefore, in these two cases, the ΔV is determined by Eq. (12).

III. Numerical results

In this specific context, numerical assessments have been conducted across diverse scenarios, encompassing a comprehensive spectrum of values for eccentricity and semimajor axis to optimize ΔV. As expounded upon in the antecedent section, Eq. (2) may yield a solution or not for the semimajor axis, a_t, and the eccentricity, e_t, contingent upon the initial conditions of both the initial and final orbits. Consequently, it becomes feasible to delineate a specific region within the system of partial differential equations concerning these variables, a_t and e_t.

A. Optimal region

We consider several values in each studied configuration in previous sections and therefore, the function to estimate is evaluated in a wide region where the ΔV should be optimal. In order to perform a numerical analysis of these configurations, we taking into account the sets of orbital elements, σ_{O_1}, σ_{O_2}, σ_{O_3}, and σ_{O_4} for the initial orbits, and σ_{O_f} for the final orbit, as given in Table 1, which e_i, i_i, Ω_i, ω_i and ν_i are same for the four configurations.

Table 1 Sets of orbital elements: Initial, σ_{O_i}, and final, σ_{O_f}, orbits.

Sets	a_i [km]	e_i	i_i [deg]	Ω_i , [deg]	ω_i [deg]	ν_i [deg]
σ_{O_1}	7000.0					
σ_{O_2}	14000.0	0.5	1.5	45.89	142.19	10.24
σ_{O_3}	28000.0					
σ_{O_4}	42000.0					
	a_f [km]	e_f	i_f [deg]	Ω_f [deg]	ω_f [deg]	ν_f [deg]
σ_{O_f}	50000.0	0.6	4.5	15.0	190.10	20.0

Figure 8 shows four contour maps of the ΔV for the first configuration calculated from Eq. (4), Eq. (5) and Eq. (6). Contour maps display different level curves of the eccentricity, e_t, with respect to the semimajor axis a_t, in km. Each set of orbital elements represents a contour map, such as: σ_{O_1} and σ_{O_f} located at the upper left, σ_{O_2} and σ_{O_f} at the upper right, σ_{O_3} and σ_{O_f} at the lower left, and σ_{O_4} and σ_{O_f} at the lower right, respectively. The behavior of the ΔV is equivalent in each scenario and is limited by level curves. Specifically, in the white, yellow and red regions it is more expensive, while in the blue regions it is cheaper, especially in the dark blue, where the optimum is found. The latter is available in a range of feasibility both in eccentricity and semimajor axis (see Fig. 8).

Therefore, the optimal ΔV are less that 1.0 km/s, 1.2 km/s, 1.8 km/s and 1.5 km/s, respectively, as shown in Fig. 8. This confers an advantage, as varying sets of orbital elements are viable for achieving the same optimal value in the

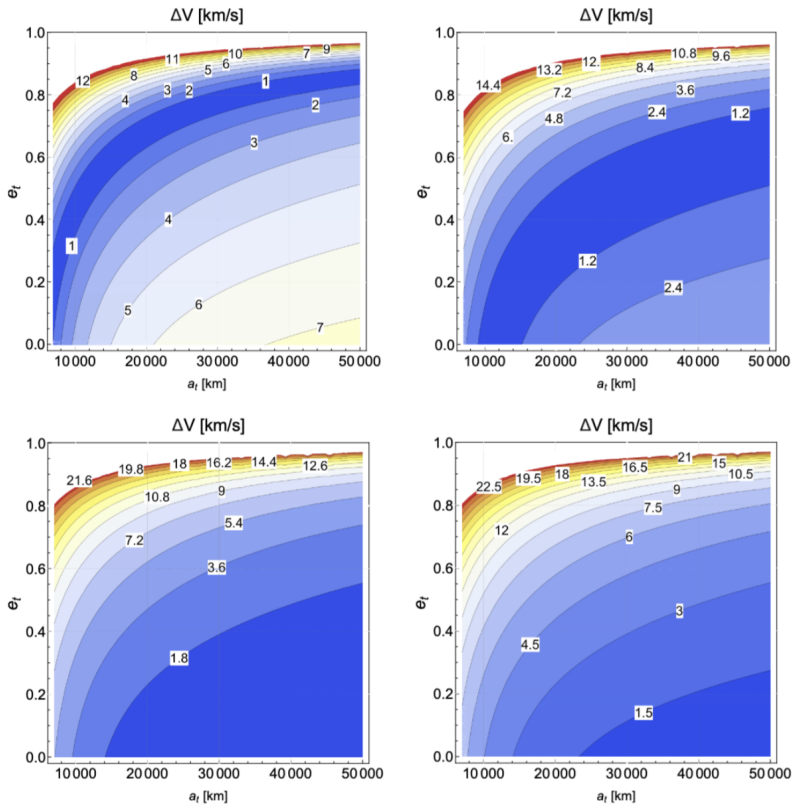

Fig. 8 Contour maps of the ΔV for the first configuration.

transfer orbit. Fig. 9 shows contour maps, taking into account the second configuration. On the other hand, Fig. 10 shows contour maps obtained for the third configuration. As indicated in Sec II. D, the behavior is similar to the fourth configuration, and the calculation of ΔV is obtained by evaluating Eq. 12; therefore, we only consider the third configuration. For each configuration the ΔV optimal values (dark-blue region) are obtained in different intervals of possible values, for e_t and a_t. Nevertheless, the behavior is equal and systematic in all cases. In order to compute the intervals of e_t and a_t with the optimal value, we determine a parametric function based on the level curves.

B. Parametric function for the ΔV

The parametric function is computed within a region bounded by the level curves where ΔV is minimized. Considering the first configuration and referring to the contour map in the upper-left of Fig. 8, we observe that e_t and a_t fall within the ranges of $e_t \in [0.0001,\ 0.84]$ and $a_t \in [6910.0,\ 50000.0]$, in km, respectively. Additionally, the optimal ΔV is determined to be $1.0, \mathrm{km/s}$. In order to derive the parametric function, the Levenberg-Marquardt method [31, 32] has been iteratively applied to determine the coefficients of the function that optimally represents the data for $\Delta V = 1$

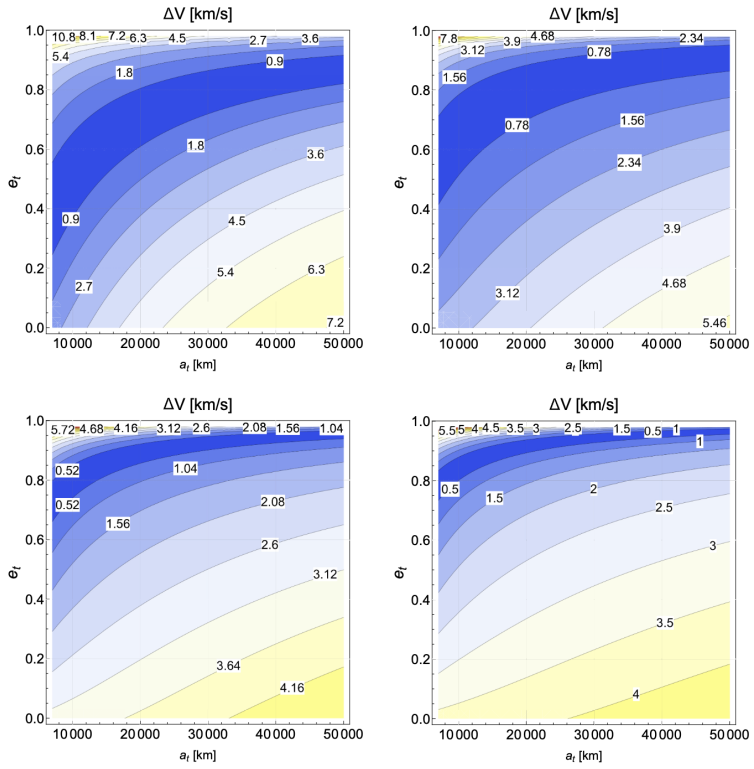

Fig. 9 Contour maps of the ΔV for the second configuration.

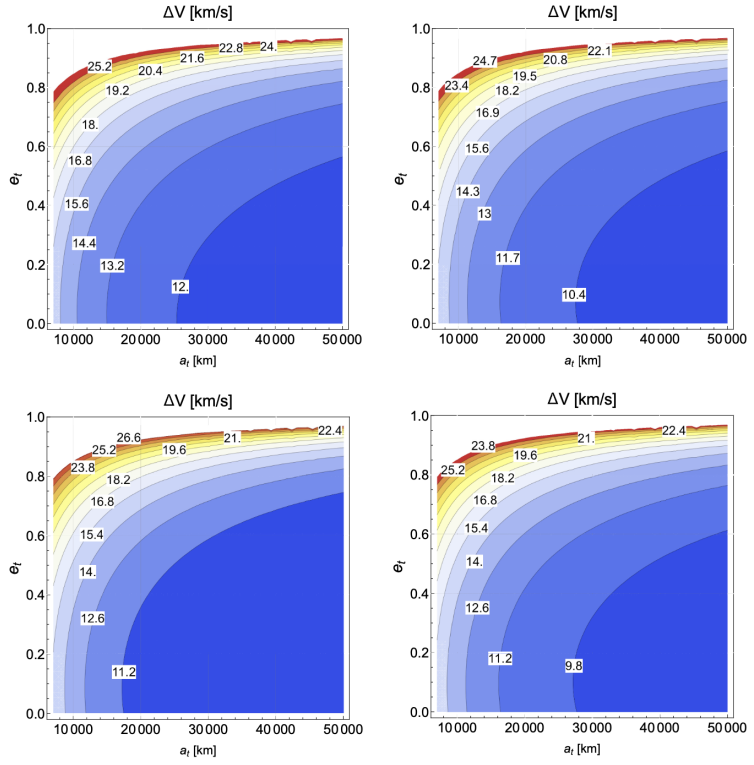

Fig. 10 Contour maps of the ΔV for the third configuration.

km/s within the selected configuration.

Following the application of the method, the chosen function corresponds to the optimal fit, as evidenced by the convergence of mean squared errors to zero. In the lower right panel of Fig. 11, standardized residuals are depicted in relation to the fitted values. It is evident that these residuals approach zero as the iterative process progresses. Notably, at iteration 60, the residuals closely approximate zero. Moreover, stability persists up to iteration 120, during which the residuals consistently maintain values between $\pm 5 \times 10^{-4}$.

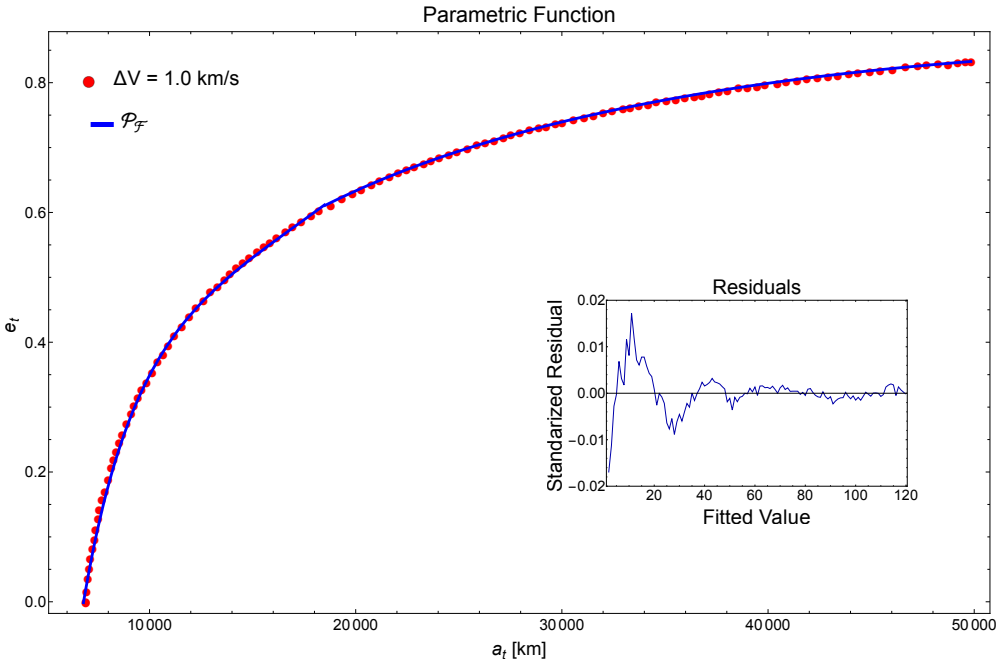

Fig. 11 Parametric function for $\Delta V = 1.0$ km/s, and residual.

Figure 11 shows the parametric function (blue line) with the optimal value of 1.0 km/s within the specified intervals for each variable. Additionally, the red points represent the calculated values obtained from the ΔV function. This function represents the eccentricity in terms of the semimajor axis of the transfer orbit. In each case, we calculate a parametric function defined in a width range of feasible values of the two unknown variables and an optimal constant value of the ΔV. The analytic parametric function, $\mathcal{P}_{\mathcal{F}}$, is defined as:

$$\mathcal{P}_{\mathcal{F}} = \begin{cases} c_0 + c_1\, a_t + c_2\, \log(a_t) + c_3\, \log(c_4 + a_t), & a_{t_i} \leq a_t \leq a_{t_1}. \\ c_5 + c_6\, a_t + c_7\, \log(a_t), & a_{t_1} < a_t \leq a_{t_f}. \end{cases} \tag{15}$$

where, c_0, c_1, c_2, c_3, c_4, c_5, c_6 and c_7 are real coefficients. The a_{t_i}, a_{t_1} and a_{t_f} are the lowest and highest values of the intervals where the function is continuous and differentiable. The log function corresponds to the natural logarithm.

The specified intervals are as follows: a_{t_i} = 6915.0 km, a_{t_1} = 18500.0 km, and a_{t_f} = 49850.0 km. The associated coefficients, along with their corresponding standard errors—defined as the square root of the reduced chi-square statistic—and the confidence intervals, are presented in Table 2, respectively. In general, the parametric function $\mathcal{P}_{\mathcal{F}}$

Table 2 Parameter Confidence Interval table.

Par	Estimate	SE	CI
c_0	24.31	3.6×10^{-2}	$\{ 22.45,\ 26.12 \}$
c_1	9.36×10^{-6}	1.49×10^{-6}	$\{ 6.4 \times 10^{-6},\ 1.2 \times 10^{-5} \}$
c_2	−67719.6	3.2×10^{-3}	$\{ -67719.6, -67719.5 \}$
c_3	67717.1	1.6×10^{-3}	$\{ 67716.8, 67719.5 \}$
c_4	-3.32×10^{-2}	2.1×10^{-3}	$\{ -3.5 \times 10^{-2},\ -2.7. \times 10^{-2} \}$
c_5	$-3.18 \times 10^{\ 0}$	$2.6 \times 10^{\ 0}$	$\{ -8.33,\ 1.98 \}$
c_6	-5.43×10^{-6}	8.6×10^{-6}	$\{ -2.2 \times 10^{-6},\ 1.1. \times 10^{-5} \}$
c_7	3.96×10^{-2}	2.7×10^{-2}	$\{ -1.5 \times 10^{-2},\ 9.4. \times 10^{-2} \}$

enables us to delineate the geometry of the transfer orbit by considering an optimal characteristic velocity based on the orbital elements of the initial and final orbits. It is noteworthy that the ΔV function demonstrates sensitivity to the initial conditions and requires a more detailed study.

C. Results

We select several sets of orbital elements for the initial and final orbits, acquired from the database `http://www.space-track.org/`. These sets represent the orbital motion of cataloged orbiters. In a previous process, these were changed from the Two Line Elements (TLE) format to classical orbital elements, with respect to the Geocentric Reference Frame. The TLE orbit is a first-order approximation to the solution of the orbital motion and is calculated under a non- orbital model.

Table 3 shows in the first column the satellite catalog number, NORAD ID and in the second one, the set of orbital elements that correspond to the initial and final orbit, σ_O. And finally, the next six columns represent the semimajor axis, a (in km), eccentricity, e, inclination, i (in deg), right ascension of the ascending node, Ω (in deg), argument of perigee, ω (in deg), and true anomaly, ν (in deg), respectively.

After considering the sets of orbital elements in each case and performing a numerical evaluation of the parametric function, we obtain the data shown in Table 4. Eight real coefficients, c_i, of the parametric function that determine the intervals for eccentricity e_t, and the semimajor axis, a_t in km, and the optimal value of the characteristic velocity, ΔV in

Table 3 Cataloged orbiters with their set of orbital elements.

NORAD ID	Set	a [km]	e	i [deg]	Ω [deg]	ω [deg]	ν [deg]
1964	σ_{O_i}	7202.38	0.01933	32.19	45.89	142.19	29.24
	σ_{O_f}	10200.00	0.02000	52.19	65.00	170.10	60.00
2643	σ_{O_i}	17449.77	0.61740	25.89	353.82	81.94	339.59
	σ_{O_f}	30000.00	0.02000	70.00	30.00	120.00	70.00
2646	σ_{O_i}	40050.14	0.00370	05.25	56.43	72.86	323.83
	σ_{O_f}	47000.00	0.01200	50.00	70.50	80.00	350.45

km/s. The values in the second, third, and fourth columns, denoted as NORAD 1964, NORAD 2643, and NORAD 2646, respectively, correspond to each analyzed case. These columns primarily present the potential values for both eccentricity and the semimajor axis of the transfer orbit, as well as the coefficient of the parametric function.

Table 4 Results after performing a numerical evaluation of the parametric function, for the three cataloged orbiters.

Par	NORAD 1964	NORAD 2643	NORAD 2646
c_0	-10.59	-5.21	-66.97
c_1	-6.36×10^{-6}	-9.61×10^{-6}	-1.28×10^{-5}
c_2	-2.73	0.0	0.0
c_3	3.96	0.59	6.78
c_4	0.43	-0.38	$-.98$
c_5	-2.57	-4.10	-28.59
c_6	-8.07×10^{-7}	-5.19×10^{-6}	-4.18×10^{-6}
c_7	0.29	0.47	2.86
a_{t_i} [km]	9065.0	7614.0	40670.0
a_{t_1} [km]	16114.5	28036.5	47689.9
a_{t_f} [km]	45150.0	45090.1	50190.3
e_{t_i}	0.00055	0.0008323	0.0006013
e_{t_f}	0.5476	0.7151	0.2344
ΔV [km/s]	1.5	1.2	3.36

IV. Conclusions

Modifying the trajectory in space of any orbiter usually require the best possible precision to achieve the success of any mission. We can design different orbits, however, the presence of many orbiters, such as space debris that can endanger any space mission, makes it often necessary to change such designs. Therefore, it has become essential and unavoidable to apply impulsive maneuvers, which in turn are restricted by a set of requirements. In this Note, we

present a fundamental function in each of the three scenarios studied in the model formulation. All of these scenarios share a feature: the transfer orbit is coaxial with either O_i or O_f. A specific function is derived with respect to the semimajor axis and eccentricity of the orbital transfer. Several sets of orbital elements which have been taken from `http://www.space-track.org/`, are used to evaluate the ΔV and illustrate the different configurations, being the second configuration the most efficient according to the general formulation and restrictions. On the other hand, we have computed, for various instances of orbital transfers, an optimal range where the ΔV is minimized. This computation involves a parametric function, facilitating the determination of intervals for both the eccentricity and semimajor axis of the transfer orbit. Within these intervals, the ΔV is consistently minimized or falls within the computed optimal region.

V. Acknowledges

This work has been supported by Grant PID2020−117066−GB−I00 funded by MCIN/AEI/ 10.13039/501100011033 and by the Aragón Government and European Social Fund (E24_23R). Special thanks go to the DOPC: Sky Quality Group (GCC)−Telescope Operation Group (GOT), of the CEFCA Foundation.

References

[1] Klinkrad, H., "DISCOS - ESA's database and information system characterising objects in space," *Advances in Space Research*, Vol. 11, No. 12, 1991, pp. 43–52. https://doi.org/https://doi.org/10.1016/0273-1177(91)90541-Q.

[2] Lemmens, S., and Letizia, F., "ESA's annual space environment report," *Space Debris Office, GEN−DB−LOG−00288−OPS−SD*, ESA/ESOC, Darmstadt, Germany, 2021, pp. 1–120.

[3] Schildknecht, T., Musci, R., Ploner, M., G, B., Flury, W., Kuusela, J., de Leon Cruz, J., and de Fatima Dominguez Palmero, L., "Optical observations of space debris in GEO and in highly−eccentric orbits," *Advances in Space Research*, Vol. 34, No. 5, 2004, pp. 901–911. https://doi.org/https://doi.org/10.1016/j.asr.2003.01.009.

[4] Flohrer, T., Schildknecht, T., Musci, R., and Stöveken, E., "Performance estimation for GEO space surveillance," *Advances in Space Research*, Vol. 35, 2005, pp. 1226–1235. https://doi.org/10.1016/j.asr.2005.03.101.

[5] Silha, J., Schildknecht, T., Hinze, A., Flohrer, T., and Vananti, A., "An optical survey for space debris on highly eccentric and inclined MEO orbits," *Advances in Space Research*, Vol. 59, No. 1, 2017, pp. 181–192. https://doi.org/https://doi.org/10.1016/j.asr.2016.08.027.

[6] Pardini, C., and Anselmo, L., "Evaluating the impact of space activities in low earth orbit," *Acta Astronautica*, Vol. 184, 2021, pp. 11–22. https://doi.org/10.1016/j.actaastro.2021.03.030.

[7] Mark, C. P., and Kamath, S., "Review of Active Space Debris Removal Methods," *Space Policy*, Vol. 47, 2019, pp. 194–206. https://doi.org/https://doi.org/10.1016/j.spacepol.2018.12.005.

[8] Nishida, S.-I., and Kawamoto, S., "Strategy for capturing of a tumbling space debris," *Acta Astronautica*, Vol. 68, No. 1, 2011, pp. 113–120. https://doi.org/https://doi.org/10.1016/j.actaastro.2010.06.045.

[9] Hohmann, W., *Die Erreichbarkeit der Himmelskörper: Untersuchungen über das Raumfahrtproblem*, De Gruyter, 1925.

[10] Shternfeld, A., *Soviet Space Science*, Basic Books, New York, 1959.

[11] Edelbaum, T., "Some Extensions of the Hohmann Transfer Maneuver," *ARS DIARIO*, Vol. 29, No. 11, 1959, pp. 864–865.

[12] Hoelker, R. F., and Silber, R., "The Bi-Elliptical Transfer Between Coplanar Circular Orbits," *Proceedings of the 4th Symposium on Ballistic Missiles and Space Technology*, Vol. 3, 1961, pp. 164–175.

[13] Ting, L., "Optimum Orbital Transfer by Impulses," *ARS Journal*, Vol. 30, 1960, pp. 1013–1018.

[14] Ting, L., "Optimum Orbital Transfer by Several Impulses," *Acta Astronautica*, Vol. 6, 1960, pp. 256–265.

[15] Lawden, D. F., "Optimal Powered Arcs in an Inverse Square Law Field," *ARS Journala*, Vol. 31, 1961, pp. 566–568.

[16] Lawden, D. F., *Optimal Trajectories for Space Navigation*, Butterworths, London, 1963.

[17] Barrar, R. B., "An Analytic Proof that the Hohmann-Type Transfer is the True Minimum Two-Impulse Transfer," *Acta Astronautic*, Vol. 9, No. 1, 1963, pp. 1–11.

[18] Marec, J.-P., *Optimal Space Trajectories*, Elsevier, Amsterdam, 1979.

[19] Battin, R. H., *An Introduction to the Mathematics and Methods of Astrodynamics*, AIAA Education Series, USA, 1999.

[20] Palmore, J. I., "An Elementary Proof the Optimality of Hohmann Transfers," *Journal of Guidance, Control, and Dynamics*, Vol. 7, No. 5, 1984, pp. 629–630. https://doi.org/https://doi.org/10.2514/3.56375.

[21] Prussing, J. E., "Simple proof of the global optimality of the Hohmann transfer," *Journal of Guidance, Control, and Dynamics*, Vol. 15, No. 4, 1992, pp. 1037–1038. https://doi.org/https://doi.org/10.2514/3.20941.

[22] Moyer, H. G., "Minimum impulse coplanar circle-ellipse transfer," *AIAA Journal*, Vol. 3, No. 4, 1965, pp. 723–726. https://doi.org/https://doi.org/10.2514/3.2954.

[23] Pontani, M., "Simple Method to Determine Globally Optimal Orbital Transfers," *Journal of Guidance, Control, and Dynamics*, Vol. 32, No. 3, 2009, pp. 899–914. https://doi.org/https://doi.org/10.2514/1.38143.

[24] Zee, C.-H., "Effect of finite thrusting time in orbital maneuvers," *AIAA Journal*, Vol. 1, No. 1, 1963, pp. 60–64.

[25] Robbins, H. M., "An analytical study of the impulsive approximation." *AIAA Journal*, Vol. 4, No. 8, 1966, pp. 1417–1423.

[26] Nelson, S. L., and Zarchan, P., "Alternative approach to the solution of Lambert's problem," *Journal of Guidance, Control, and Dynamics*, Vol. 15, No. 4, 1992, pp. 1003–1009. https://doi.org/https://doi.org/10.2514/3.20935.

[27] Vallado, D., *Fundamentals of Astrodynamics and Applications*, 3th edition, Springer, Berlín, 2007.

[28] Thompson, B. F., and Rostowfske, L. J., "Practical Constraints for the Applied Lambert Problem," *Journal of Guidance, Control, and Dynamics*, Vol. 43, No. 5, 2020, pp. 967–974. https://doi.org/https://doi.org/10.2514/1.G004765.

[29] Quarta, A., and Mengali, G., "Simple solution to optimal cotangential transfer between coplanar elliptic orbits," *Acta Astronautica*, Vol. 155, 2019, pp. 247–254. https://doi.org/https://doi.org/10.1016/j.actaastro.2018.12.007.

[30] Abad, A., *Astrodinámica*, Bubok Publishing S.L., 2012.

[31] Levenberg, K., "A Method for the Solution of Certain Non-Linear Problems in Least Squares," *Quarterly of Applied Mathematics*, Vol. 2, 1944, pp. 164–168. https://doi.org/https://doi.org/10.1090/qam/10666.

[32] Behling, A., R. Fischer, "A unified local convergence analysis of inexact constrained Levenberg–Marquardt methods," *Optimization Letters*, Vol. 6, 2012, pp. 927–940. https://doi.org/https://doi.org/10.1007/s11590-011-0321-3.